Rocket Thrust Perturbation from Discharge of an Inert Body

John W. Murdock*
The Aerospace Corporation, El Segundo, California

Measured thrust-time histories of solid rocket motors frequently have perturbations or excursions about some nominal value. One cause of these perturbations and the subject of this paper is the expulsion of an inert mass, e.g., an igniter that has come loose. The objective of this work was to numerically generate accurate, high time-resolution thrust curves for various idealized cases of mass discharge to improve the understanding of this phenomenon. Although the thrust perturbation is usually negative when the ejected body blocks the nozzle throat, the total impulse associated with mass ejection is always positive. Also, the positive thrust perturbation associated with the ejection may be present long after the body has exited the nozzle.

Nomenclature

a	= acceleration
A	= area
c^*	= characteristic velocity, Eq. (A4)
C	= integration constant, Eq. (A9)
f	= function of γ, Eq. (A3)
H	= stagnation enthalpy
L	= length
m	= mass
n	= burn rate exponent
p	= pressure
r	= radius
R	= gas constant
R_1, R_2	= Riemann variables
t	= time
T	= thrust
T_c	= chamber temperature
u, v	= axial and radial velocity, respectively
V	= volume
γ	= specific heat ratio
ρ	= density
τ	= time constant, Eq. (A6)

Subscripts

b	= burn surface property
B	= body property
c	= chamber property
t	= throat property
0	= reference value
1,2,3	= constant state regions adjacent to the burn surface (Fig. 2)

I. Introduction

IN the spring of 1983, the second-stage solid rocket motor of the Inertial Upper Stage (IUS) failed in flight prior to the completion of motor burn. This failure resulted in extensive studies to identify the cause of the problem so that it could be corrected on future flights. One of the failure scenarios postulated that the thrust perturbation (starting at 74 s in Fig. 1), which occurred about 10 s prior to the failure, was caused by the ejection of an inert mass. It was also postulated that this inert mass damaged the nozzle interior in the process of being discharged, leading to the later failure. Thus, the initial objective for this work was to determine the likelihood of the thrust perturbation in Fig. 1 being caused by inert mass ejection.

It is not possible to obtain a fundamental understanding of the thrust perturbation caused by mass ejection by inspecting static test data. Only an occasional motor will eject an inert mass. Furthermore, since the source of this mass is usually some type of failure, the geometry and even the precise number of objects are unknown. It might be possible to circumvent these obstacles if it were not for the fact that the time resolution of the thrust measurement is (in all data available to this author) inadequate to resolve the very rapid mass ejection.

A search of the literature at the start of this work turned up no fundamental work on this subject; therefore, an unsteady, axisymmetric, numerical simulation of mass ejection was made to identify the relevant time scales and important parameters governing this problem. Just before this paper was submitted for publication, a study of the effects of inert mass ejection on combustion instability of rocket motors was published.[1] However, this study does not specifically address the thrust perturbation question which, to the author's knowledge, is considered in detail for the first time in this paper.

II. Analytical and Numerical Model

A means for predicting the thrust-time history of a solid rocket motor ejecting a given inert mass is needed. In order to make this problem tractable, several assumptions have been made. Consideration is restricted to unsteady, axisymmetric flow. Consistent with this assumption, the ejected bodies are restricted to flat-faced cylindrical bodies whose axes are coincident with the nozzle axis. Thus, the bodies are completely specified by their mass (or density), length, and diameter.

The flow in the rocket motor is assumed to be that of an inviscid, perfect gas with a constant ratio of specific heats. The assumption of a perfect gas is only approximate for a solid rocket motor; however, it is deemed adequate here since the primary interest is the perturbation about some nominal caused by mass ejection. All of the numerical calculations presented herein use $\gamma = 1.135$; approximate techniques to treat other nozzles and flow properties are also given. The neglect of viscosity is an adequate assumption for the baseline nozzle flow. The inviscid approximation does preclude

Received May 10, 1985; revision received Nov. 29, 1985.

*Engineering Specialist, Fluid Mechanics Department. Associate Fellow AIAA.

viscous, boundary-layer drag on the side of the cylindrical bodies but does predict flow separation at the aft end of the bodies. For the flat-faced cylinders treated herein, the drag resulting from the pressure difference between the fore and aft faces exceeds the viscous boundary-layer drag by as much as three orders of magnitude. Thus, the inviscid assumption is deemed satisfactory. Similarly, it is expected that any body actually ejected by a rocket motor due to a mechanical failure would be nonstreamlined with a trajectory controlled by pressure forces.

The unsteady, axisymmetric Euler equations are used to model this problem. These equations are solved using the Godunov cell method.[2] A computer code which has evolved and been improved upon for more than 10 years[3,4] was tailored to treat the mass ejection problem. The mass fluxes at the cell boundaries in the Godunov code are obtained by analogy with a shock tube. In the current version of the code, the nonlinear Riemann equations are solved to obtain cell fluxes; this is an improvement over earlier versions that used the acoustic (linearlized) version of the Riemann equations. The nonlinear version gives an accurate and numerically stable treatment of strong shocks and rarefaction waves. The main disadvantage of the Godunov code is that it is first-order accurate; it also smears out discontinuities such as shocks and contact surfaces. The main advantage of the method is its versatility; any inviscid gasdynamic problem can be treated as long as the explicit Courant stability limit on the time step is not violated. For the present problem, the use of the Godunov code is considered to be adequate, particularly in light of the fact that the primary interest is in an integral quantity—the nozzle thrust—as opposed to detailed local flowfield information.

The treatment of the solid-rocket-motor burning-surface boundary condition and the passage of a solid body through a fixed Eulerian mesh required specific modifications to the existing Godunov code. These modifications will be described herein.

In an actual solid motor, the burning surface—the ultimate source of the nozzle flow—recedes with time. The subject of this report is inert mass ejection; and consistent with this subject, the receding burn surface is expected to be of negligible physical importance and has been replaced with a fixed source at the outer radius of the combustion chamber. The stagnation enthalpy of the combustion gas is assumed to be constant in time

$$H = \text{const} = \gamma p_3/[(\gamma-1)\rho_3] + 0.5v_3^2 \qquad (1)$$

at the burn surface, as shown in the wave diagram in Fig. 2. The mass flow rate at the surface is a function of the pressure and a burn rate exponent.

$$\rho_3 v_3 = -\rho_0 v_0 (p_3/p_0)^n \qquad (2)$$

For the results presented herein, a value of $n=0.4$ has been used. Note, however, that the variation of mass flow with pressure in Eq. (2) is weak; thus, to a first approximation, the burn surface acts as a mass source independent of pressure. Equations (1) and (2) are two equations for three unknowns and, therefore, do not determine p_3, ρ_3, and v_3. This is as expected for subsonic boundary conditions. The final relation is obtained by treating the boundary in a manner consistent with the Godunov treatment[2] of internal cell boundaries, i.e., formulating a Riemann problem. The appropriate Riemann problem is shown in Fig. 2, in which a left-running acoustic wave and a contact surface emanate from the boundary at each time step. The Riemann variable

$$R_1 = R_2 = 2[(\gamma p_i/\rho_i)^{0.5}]/(\gamma-1) + v_i, \qquad i=1,2 \qquad (3)$$

is constant along right-running waves and, hence, is constant across the left-running wave (in regions 1 and 2). Equations (1-3), plus the fact that both the velocity and pressure are constant across the contact surface ($p_2=p_3$; $v_2=v_3$), are sufficient to determine boundary (region 3) properties. (Region 1 properties are cell-centered and are known at the start of the time step.)

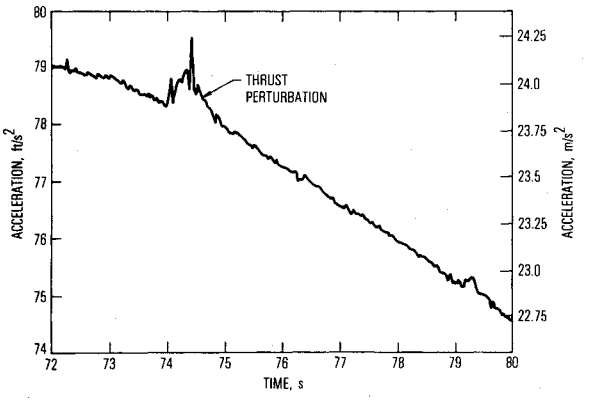

Fig. 1a IUS acceleration time history.

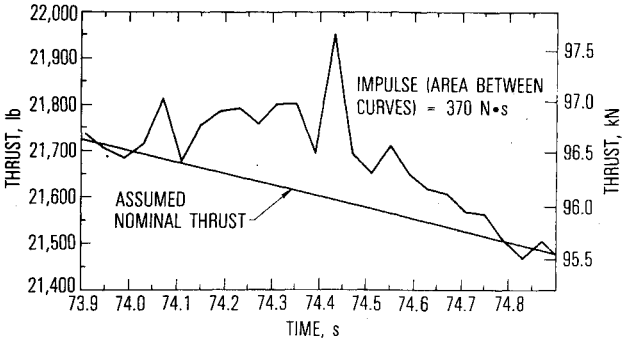

Fig. 1b IUS thrust-time history.

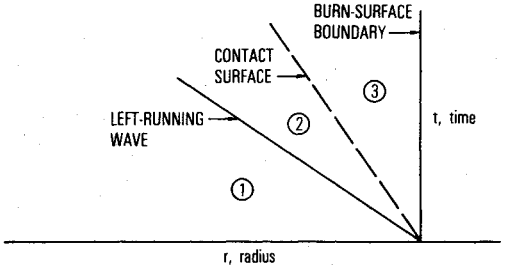

Fig. 2 Burning-surface Riemann problem.

Some special logic was required in the Eulerian, Godunov code in order to treat a solid body moving through the nozzle. The radius of the body was always chosen to be on a cell boundary; thus, knowing the axial location of the body, one can either compute the radial mass, momentum, and energy fluxes normally or call a standard solid boundary routine, as appropriate at $r=r_B$. The axial direction is more complicated because the body moves into cells in front of it and out of cells behind it.

A modification of the Eulerian grid fore and aft of the body was required to prevent the stable time step from becoming too small. To see how this can occur, consider a cell that the body takes several time steps to engulf. As the body advances and the gas volume of the cell decreases, the stable time step associated with this cell also decreases proportionately. Thus the lower limit on the time step is zero, which is unacceptable. To avoid this problem, the two cells immediately in front and immediately behind the body are

combined and treated as one. When cells are combined, their properties are mass-averaged. In this way, the body moves into a cell with an axial length varying between 1 and 2 cell lengths rather than 0 and 1 cell lengths; therefore, there is no time-step reduction associated with the passage of the body. Once the logic is in place to generate the special cells fore and aft of the body, the other changes are straightforward. A moving solid boundary differs from a stationary one in one respect only: in the former case, work is done on the fluid. The total force on the body is computed by integrating the pressure force at each time step. A first-order Euler integration scheme, comparable in accuracy to the basic Godunov code, integrates the force (or acceleration) on the body to compute velocity and axial location as a function of time.

III. Calculation Procedure

There are three steps in determining the thrust perturbation associated with mass ejection. First, the steady or nominal thrust must be computed to enough significant figures to be able to resolve the small thrust perturbation about the nominal. The second step is to compute the thrust-time history of the motor during the time period when the ejected body is within the motor. The final step entails determining the thrust perturbation caused by the ejected body but occurs after the body has departed the nozzle.

In principle, since the Godunov code is an unsteady code, one could start with some arbitrary initial condition and run until steady flow in the motor is achieved. As will be shown, this procedure is too costly in terms of computer time, and a modification is required. Starting with the desired initial pressure and density in the combustion chamber, the numerical computation is run until the numerical solution tracks the quasisteady, analytical blowdown solution given in the Appendix and all other unsteady effects have been damped out. One such steady effect, which is easily excited but also quickly damps, is the acoustic resonance of the combustion chamber. (The pressure oscillation is caused by axial acoustic waves in the chamber; this has been shown by comparing the oscillation period with the time required for a sound wave to traverse the chamber length twice.)

To demonstrate that running the unsteady flow code through the blowdown transient is not a viable way to achieve a steady solution, a comparison of the code time step and the blowdown time can be made. A typical code time step is on the order of 20 μs, while the rocket motor time constant τ has a value of order 0.1 s for most cases considered herein. The pressure decay is given by Eq. (A8); the decay rate is controlled by both τ and the burn rate exponent, n. The characteristic pressure decay time is actually a factor of 2 or 3 times τ. Therefore, it would take tens of thousands of time steps for the numerical simulation to relax to absolutely steady flow. Code execution time on the CDC 176 is about 3.8 s per time step. Thus, achieving steady flow by brute-force running of the code is prohibitively expensive.

To circumvent this problem, convergence to a steady solution is accelerated by making a minor adjustment to the constant v_0 appearing in Eq. (A2). This adjustment is such that the numerically integrated mass flow into the chamber exactly equals the numerically integrated outflow through the throat and, therefore, the unsteady mass accumulation in the chamber is zero. Once the numerical solution follows the analytical solution in the Appendix, an adjustment to v_0 of order 0.5%, followed by a few hundred steps of computation, reliably produces steady, numerical flow. Note that the small v_0 adjustment implies that the flow must be steady to within a few tenths of a percent; absolute accuracy to that level is not required and is probably not achievable. As discussed in the next section, the accuracy of the steady solution as compared with one-dimensional flow is satisfactory.

After the steady numerical solution is obtained, the body is introduced into the combustion chamber. Figure 3 shows the chamber and nozzle geometry used for this study. (Note that the radial direction has been magnified relative to the axial direction in Fig. 3). The axial length of the combustion chamber is 579 mm, while the bodies vary in length from 51 to 203 mm. All of the bodies are introduced with an axial velocity of 3 m/s; in addition, the rocket motor is assumed to be accelerating at 2.5 g so that the body is subject to the integrated pressure force as well as the force arising from the 2.5-g acceleration. The 3-m/s initial velocity and the 2.5-g acceleration are negligible compared to the velocity of the

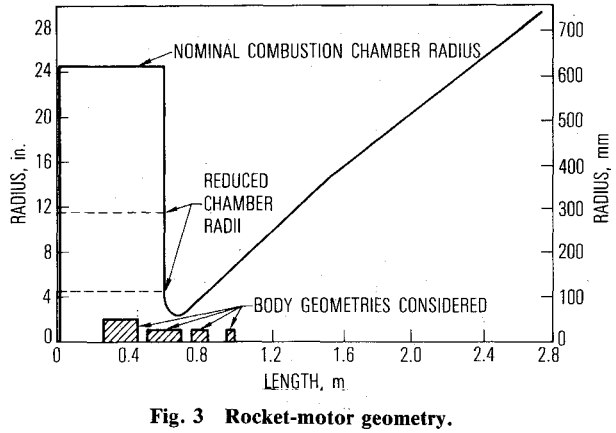

Fig. 3 Rocket-motor geometry.

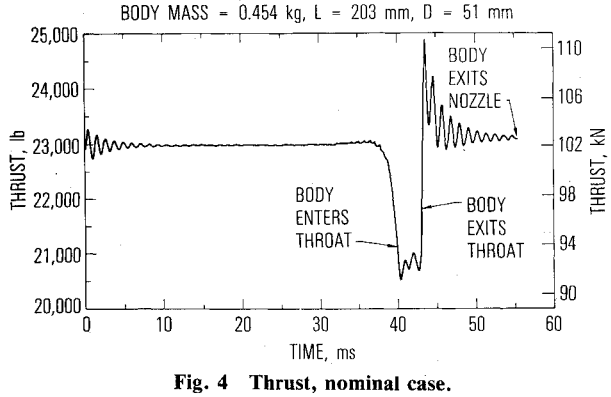

Fig. 4 Thrust, nominal case.

Table 1 Mass ejection parameters

Body mass, kg	Body length, mm	Body diameter, mm	Body density, (Mg/m^3)	Impulse, N·s	Impulse/ mass, m/s	Exit velocity, m/s
5.70	203	102	3.32	654	115	88.4
1.43	203	51	3.32	141	99.4	82.3
1.43	102	51	6.92	126	88.7	70.1
0.713	51	51	6.92	66.7	93.6	91.4
0.454	203	51	1.11	75.2	166	142

body downstream of the throat and the acceleration while the body traverses the throat, respectively. However, these values do affect the trajectory of the body in the combustion chamber where gasdynamic forces are small. One numerical computation was made in which the body was introduced at the forward end of the combustion chamber (5.7-kg body). It was found that no significant thrust perturbation occurred until the body approached the throat; furthermore, the code had to be run for an extended period before the body reached the throat. In subsequent computations, the body was introduced near the center of the combustion chamber to save computer time. During the time the body traverses the nozzle, the thrust, chamber pressure, velocity, and axial position of the body are monitored. The vacuum thrust is obtained by summing the axial component of the pressure force acting over the entire interior surface of the nozzle. The chamber pressure plotted herein is defined as the value halfway between the axis and the burn surface at the forward end of the combustion chamber.

The final stage occurs after the body passes through the exit plane of the nozzle. In this stage, the nozzle undergoes a quasisteady blowdown; this blowdown, which is the result of the earlier throat blockage, may take place on a time scale that is large compared to the mass ejection time. For reasons already given, this blowdown is modeled analytically (see the Appendix) rather than numerically. The chamber pressure at the time the body is discharged defines the initial condition for Eq. (A8) which, in turn, determines the subsequent nozzle behavior.

IV. Numerical Results

The majority of the numerical calculations performed for this report used the nominal combustion chamber shown in Fig. 3. The dimensions of this chamber are: radius, 622 mm; axial length, 597 mm. The nozzle throat radius is 57.2 mm, and the exit plane radius is 718 mm for an area ratio of 158. The steady flow stagnation pressure and density are, respectively, 5.04 MPa and 5.00 kg/m^3.

When a specific heat ratio of 1.135 is used, the one-dimensional, isentropic (vacuum) thrust can be computed to be 108 kN. This value is within 5% of the steady flow thrust of 102 kN obtained with the computer code. The small difference between the two values of the thrust is assumed to be caused by the fact that the real nozzle flow is not one-dimensional. A second cause of the difference is the artificial viscosity that stabilizes the numerics and is implicit in the Godunov method. Because of the artificial viscosity, the numerically computed flow is not exactly isentropic.

Five different bodies were ejected from the nominal chamber shown in Fig. 3. The body masses and geometries are listed in Table 1 along with total impulse generated by, and the exit velocity of, the masses.

Figures 4-7 show the time history of the mass ejection event for the 0.454-kg body. The initial thrust and pressure oscillations are caused by introducing the body into the combustion chamber. These oscillations are manifestations of the resonant sound wave in the chamber, mentioned previously. The initial oscillation damps out, but the resonance mode is excited subsequently by other physical events. Aside from the initial oscillation, the thrust is relatively constant until about 30 ms. Referring to Fig. 5, the chamber pressure actually drops about 0.1% between 0 and 30 ms. There is no evidence that this very small pressure drop is caused by the presence of the mass; in retrospect, it appears that the method described in Sec. III for obtaining a steady flow was not quite adequate for the chamber pressure—at least to the much magnified scale of Fig. 5. However, the main interest herein is in the thrust-time history; to the scale of Fig. 4, the thrust between 0 and 30 ms is constant. On this basis, the flow was deemed to be steady to sufficient accuracy.

Before considering the thrust in detail, consider momentum conservation for the entire motor

$$T=\iint_{\text{exit}}(p+\rho u^2)\mathrm{d}A+\frac{\mathrm{d}}{\mathrm{d}t}(m_B u_B)+\frac{\partial}{\partial t}\iiint_{\text{motor}}\rho u\,\mathrm{d}V \tag{4}$$

where T is the vacuum thrust and $m_B v_B$ the body momentum. The first term on the right-hand side gives the usual steady flow thrust of a nozzle; this term increases with increasing chamber pressure or throat area. The second two terms sum to the time rate of change of the axial momentum in the motor. The second term is the time derivative of the body momentum and is positive during the entire traverse of the body through the motor. The final term is the derivative of the gas momentum in the motor. This term is negative when total gas momentum decreases, e.g., when the throat is blocked, and is positive when gas momentum increases, i.e., the body clears the throat. [Recall that the numerically computed thrust is obtained by integrating the pressure force on the entire interior motor surface; Eq. (4) is introduced only to aid physical understanding and to make a connection with steady flow thrust methods.]

Figure 4 depicts the thrust-time history of a nozzle blockage event that occurs on a finite time scale. To better understand this figure, consider what would happen if the nozzle were instantaneously blocked. The first term in Eq. (4) is initially unchanged by the instantaneous blockage; it changes to its new quasisteady value only after the rarefaction wave generated by the blockage reaches the nozzle exit plane. The body term jumps to its new value instantaneously. The third term is only nonzero in the time interval after the blockage and before the first term attains its new quasisteady value. Furthermore, this third term serves mainly to smooth out the rapid change in the first term. The axial momentum of the gas in the motor [third term in Eq. (4)] changes only while the rarefaction wave created by the nozzle blockage travels downstream to the nozzle exit plane.

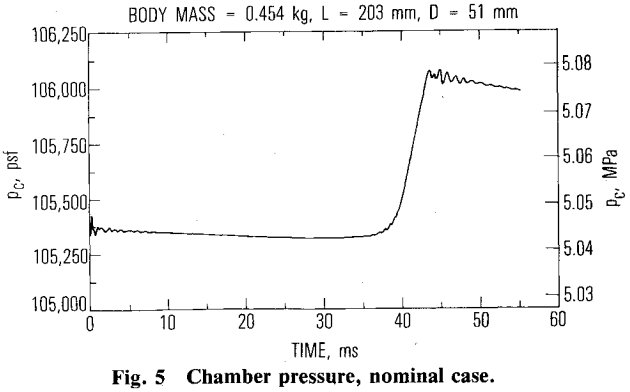

Fig. 5 Chamber pressure, nominal case.

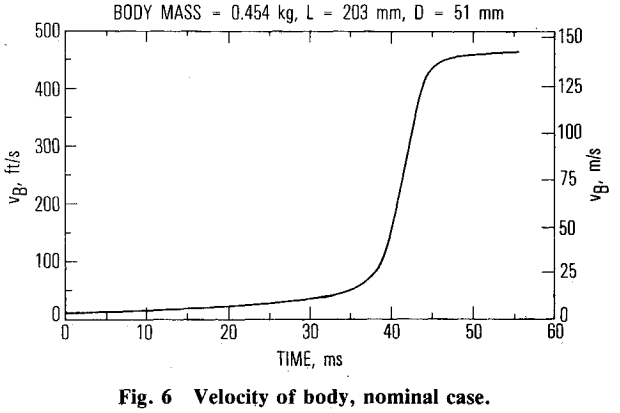

Fig. 6 Velocity of body, nominal case.

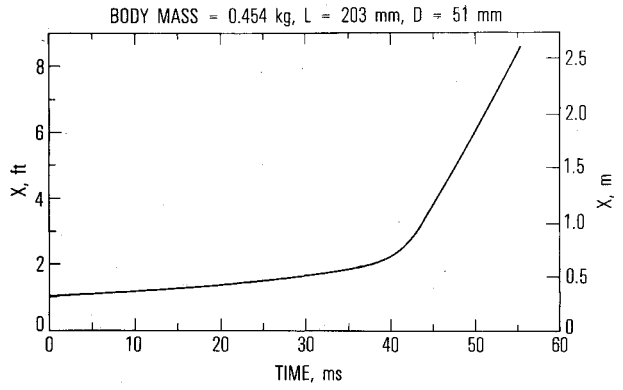

Fig. 7 Location of front of body, nominal case.

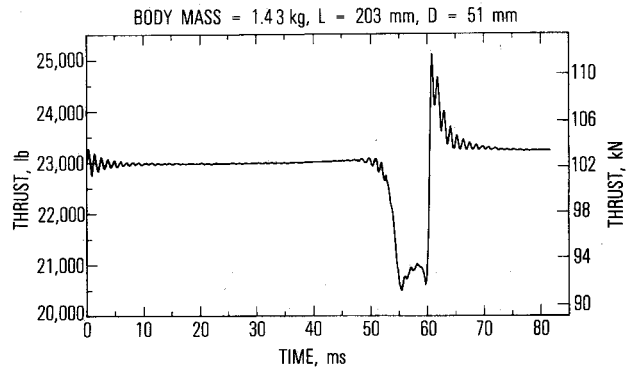

Fig. 8 Thrust, increased body mass.

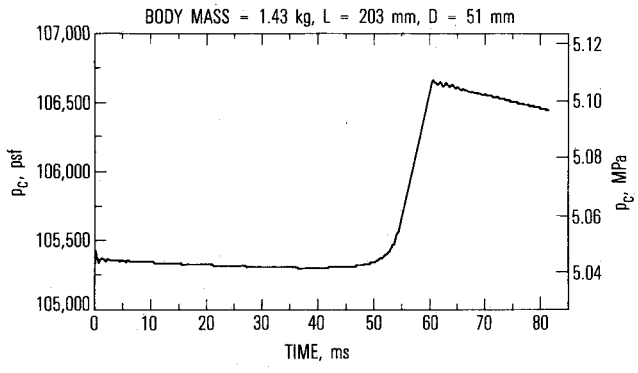

Fig. 9 Chamber pressure, increased body mass.

Once a new quasisteady flow is achieved, the unsteady term in Eq. (4) returns to zero.

Returning to consideration of the real blockage event depicted in Fig. 4, the value of the thrust for $40<t<43$ ms is interpreted as the quasisteady value associated with the throat blockage. (Inspection of Figs. 5-7 demonstrates that the body is traversing the throat in this time period.) By analogy with the previous paragraph, it is expected that the thrust in this quasisteady blockage flow region can be approximately predicted using the first two terms in Eq. (4) only. Such a comparison will be made to elucidate the physics and justify approximate methods that can be used when numerical computations are not available. The first term in Eq. (4) may be estimated by computing the steady, one-dimensional, isentropic thrust for an equivalent nozzle. Subtracting the blocked area gives a throat area of 8260 mm^2

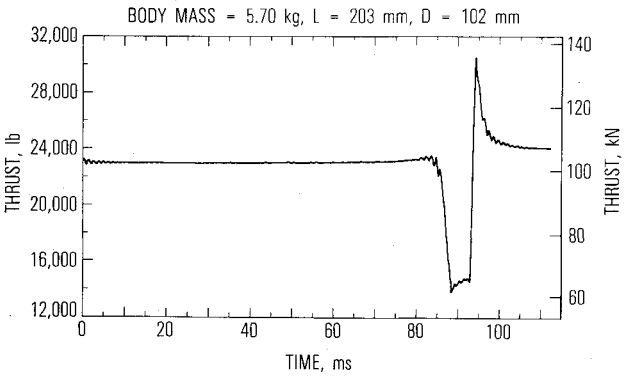

Fig. 10 Thrust, increased body radius.

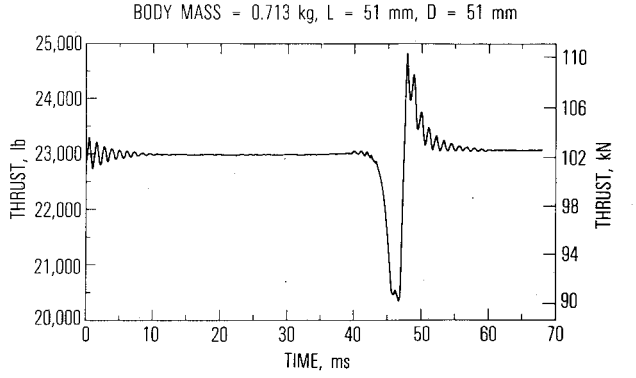

Fig. 11 Thrust, short body.

and an area ratio of 196. The thrust [first term in Eq. (4)] is computed to be $0.95\times87.4=88.2$kN. (The 5% reduction is used for consistency with the unblocked nozzle, as discussed previously.) A good value for the second term of Eq. (4) for the rather long blunt bodies considered herein is the product of the chamber pressure and the body area, in the present case 10.21 kN. Although this approximation is obviously high because the pressure in front of the body can never be zero, it is quite good. For example, the numerically computed force on the body at $t=41$ ms is 9.82 kN, only 4% lower than the estimated value. The sum of these two values is 93.4 kN, which slightly overestimates the minimum thrust in Fig. 4.

That the estimate is high is probably not surprising; the estimate for the first term in Eq. (4) is 95% of the isentopic thrust. Nonisentropic effects not accounted for by the 5% correction are: a) the blunt body in the throat does not present smooth flow contours, and b) the gas does work on the mass. Nevertheless, simple use of Eq. (4) gives a good first approximation to the minimum in Fig. 4 and aids in the physical understanding of this minimum. The duration of the minimum thrust is the time that the throat is blocked and is easily estimated using the aforementioned estimate of the body acceleration, $a_B=p_cA_B/m_B$, thus $t_{\min}=(2L_B/a_B)^{0.5}=4.3$ ms, where L_B is the body length.

The rise time of the thrust from the quasisteady minimum in Fig. 4 to the maximum is on the order of 1 ms. This is the right time scale for establishing a new quasisteady nozzle flow subsequent to the rapid unblocking of the throat. The blockage gives a chamber pressure rise of less than 1% (see Fig. 5); consequently, the postblockage, preblowdown value of the first term in Eq. (4) is 103 kN. In order to obtain the total thrust, the body acceleration term of about 10.2 kN must be added; the body acceleration remains high (Fig. 6) for 1 or 2 ms after the throat unblocks (at about $t=43$ ms) and then decays rapidly. The estimated peak thrust is 113 kN

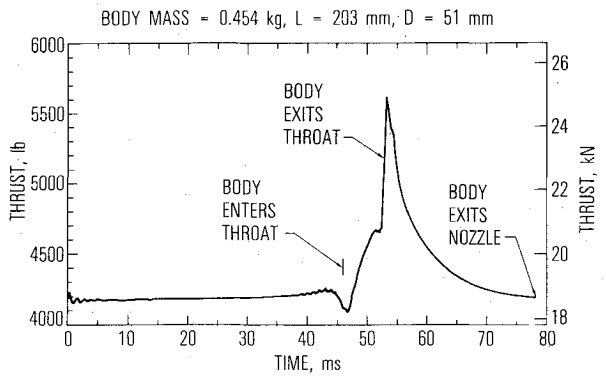

Fig. 12 Thrust, extra small chamber.

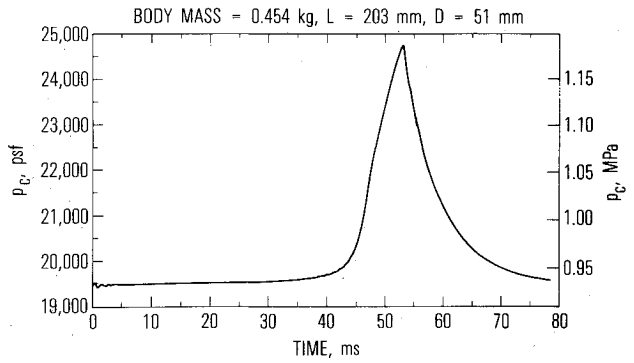

Fig. 13 Chamber pressure, extra small chamber.

compared with a value of 110 kN in Fig. 4. The peak is presumably overestimated for the same reasons that the minimum was overestimated. By 45 ms, Fig. 6 shows that the body acceleration is reduced significantly. This is consistent with the rapid thrust decay shown in Fig. 4. After the body exits the nozzle and the chamber resonance has damped, the flow is quasisteady and is modeled adequately by the equations in the Appendix.

Figures 8 and 9 show the thrust and chamber pressure histories for a body that differs from that of Figs. 4 and 5 only in that the mass has been increased by a factor of 3.14. The physical arguments presented for estimating the thrust levels are not dependent upon the body mass except for the the thrust at large times, which depends on the blockage time. A comparison of Figs. 4 and 8 shows that the numerical results support this conclusion. The amount of time that the throat is blocked—the time duration of the negative thrust perturbation— is expected to vary as the square root of the body mass. (This corresponds to a body velocity inversely proportional to the square root of the mass.) A comparison of Figs. 4 and 8, as well as the corresponding exit velocities listed in Table 1, again supports the expectation. Finally, since the burn surface acts to first order like a mass source, the chamber pressure rise and the $t > 70$-ms thrust perturbation should vary as the square root of the mass. Comparison of Figs. 4 and 5 with Figs. 8 and 9, respectively, also confirms this expectation.

Figure 10 shows the thrust-time history of a body with the same length and density as the body used to obtain Fig. 8, but with a diameter that is increased by a factor of 2. The general character of this curve is similar to that of Figs. 4 and 8. To estimate the minimum thrust in Fig. 10, an area ratio of 751 has been used to give, for the first term in Eq. (4), a value of $0.95 \times 23.9 = 22.7$ kN. As before, the body acceleration term is estimated as the product of chamber pressure and body area, 40.9 kN. The sum of these two

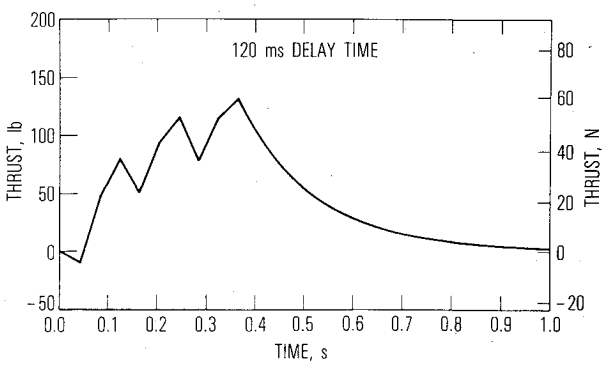

Fig. 14 Thrust perturbation, three bodies.

values, 63.6 kN, agrees well with the minimum in Fig. 10. The thrust perturbation when the body exits the nozzle has increased by a factor of 4 in Fig. 10 as compared to Fig. 8; this is in accord with the factor of 4 increase in body cross-sectional area. Addition of the postblockage thrust of 107 kN to the body acceleration gives 147 kN, which, as before, somewhat overestimates the maximum thrust.

Results presented so far have been for 203-mm-long bodies. As shown in Table 1, computations were also carried out for bodies 51 and 102 mm long. Figure 11 shows the thrust-time history for the 51-mm body. This figure shows that a body with a length-to-diameter ratio of unity behaves essentially the same as the longer bodies; also, the approximate methods already given can be used to estimate the thrust values.

One final result may be abstracted from Table 1. If one is interested only in the total impulse associated with the mass ejection event, it may be estimated to an accuracy of within 20% with only the exit momentum of the mass known. The final two columns of Table 1 show that the total impulse exceeds the exit momentum by from 2 to 20%.

In addition to the results already presented, a brief study was made to show the effects of reducing the combustion chamber volume. The numerical results have demonstrated that, for the nominal combustion chamber (Fig. 3), the blockage results in a relatively small chamber pressure rise because the volume of the chamber is large. This results in a sizeable decrease in thrust during the time the throat is blocked. Obviously, if the chamber volume is small enough, the chamber pressure rise can counteract the thrust decrease associated with throat blockage. Calculations were made with chamber radii (Fig. 3) of 292 and 114 mm to investigate this phenomenon. A 0.454-kg body, 203 mm long and 51 mm in diameter, was used to obtain these results.

The character of the thrust-time curve for the 292-mm chamber is similar to the curves already presented. In this case, the pressure rose from about 3.79 to 3.94 MPa during throat blockage. This 4% rise in pressure was not enough to overcome a 10% decrease in thrust.

Figures 12 and 13 show the thrust and pressure, respectively, for mass ejection from the 114-mm-diam chamber. In this case, the 27% increase in chamber pressure (Fig. 13) that occurs during throat blockage, is sufficient to quickly cancel the small negative thrust perturbation which occurs at the start of throat blockage. Also note that the decreased chamber volume has decreased the blowdown transient time, with the result that the thrust and pressure have essentially returned to their steady-state values when the body exits the nozzle.

V. Concluding Remarks

Several numerical simulations of mass ejection are presented herein. Comparison of these numerical results with simple models based on conservation of momentum for the rocket motor give both a better physical understanding of

the physics of the event and a basis for making approximate predictions in the future. One such result is that the exit momentum of the body is approximately equal to the impulse perturbation acting on the rocket motor.

Since this problem was originally motivated by the Inertial Upper Stage flight failure, it is appropriate to return briefly to that subject. The data in Fig. 1 are obtained from flight instrumentation that telemeters the vehicle velocity every 40 ms. From the velocity change, one can compute the 40-ms average acceleration and thrust to obtain curves such as in Fig. 1. Numerical calculations presented herein show that 40-ms time resolution is not sufficient to capture a mass ejection event which occurs in about 80 ms. To determine if thrust perturbations such as those shown in Fig. 1 could have been caused by mass ejection, Fig. 11 and its analytical extension were averaged in 40-ms intervals. Three such curves—with a 120-ms delay, simulating three masses— were summed as shown in Fig. 14. Figure 14 is similar in character to Fig. 1; however, most of the detail is lost in the averaging process. Because of this loss of detail, with a proper choice of masses and delay between them, the data in Fig. 1 could be fit to arbitrary precision. Thus, from the calculations contained herein, it can be concluded that the thrust perturbation which occurred in flight could have been caused by the ejection of several masses. However, it is not possible to rule out other causes of the thrust perturbation. Note that chamber pressure data were not available from the flight; had these data been obtained, it probably would be possible to make a more definitive statement.

Appendix: Quasisteady Chamber Pressure Decay

When a rocket nozzle discharges a mass, the combustion chamber pressure is increased above its steady flow value. The chamber pressure then decays back to its steady-state value. The time scale for this decay can be very long compared to the time for a body to traverse the nozzle length. Although, in principle, this pressure decay could be treated numerically with the computer code that is the subject of this paper, such a numerical treatment can be prohibitively expensive because of the time scales involved. Therefore, an analytical model is used to characterize the chamber pressure decay subsequent to the time the discharged mass crosses the nozzle exit plane. The analysis given herein follows a similar development given by Heister and Landsbaum.[5]

In contrast to the numerical model considered in Sec. II, the chamber pressure and density are considered to be functions only of time. In the numerical model, these quantities vary radially and axially as well as temporally. It is further assumed that the chamber temperature is constant. With these assumptions and the burn rate equation [Eq. (2)], it is possible to obtain an analytical expression for p_c as a function of time using conservation of mass for the combustion chamber.

Equation (2) gives the burn surface mass flow rate per unit area; rewriting this equation in terms of the chamber properties,

$$-\rho_c v_b A_b = \rho_0 v_0 A_b (p_c/p_0)^n \tag{A1}$$

Conservation of mass for the combustion chamber states that the time rate of change of the chamber mass equals the inflow at the burn surface minus the choked outflow through the nozzle throat.

$$V_c \frac{d\rho_c}{dt} = \rho_0 v_0 A_b \left(\frac{p_c}{p_0}\right)^n - f(\gamma) p_c A_t / (RT_c)^{0.5} \tag{A2}$$

The function f is defined as

$$f(\gamma) = (\gamma^{0.5})[2/(\gamma+1)]^{[0.5(\gamma+1)/(\gamma-1)]} \tag{A3}$$

and is related to the characteristic velocity by

$$c^* = [(RT_c)^{0.5}]/f(\gamma) \tag{A4}$$

At steady flow, the left-hand side of Eq. (A2) is zero and by definition $p_c = p_0$. Thus, the right-hand side of Eq. (A2) gives

$$v_0 A_b = f(\gamma) A_t (RT_c)^{0.5} \tag{A5}$$

Equation (A5) implicitly defines v_0.

The characteristic time

$$\tau = V/[f(\gamma) A_t (RT_c)_{0.5}] \tag{A6}$$

is the time required to discharge the total mass in the combustion chamber under steady flow conditions.

Combining Eqs. (A2), (A5), and (A6) gives

$$\frac{d(p_c/p_0)}{d(t/\tau)} = \left(\frac{p_c}{p_0}\right)^n - \frac{p_c}{p_0} \tag{A7}$$

Integration of Eq. (A7) produces

$$p_c/p_0 = \{1 + C\exp[-(1-n)t/\tau]\}^{[1/(1-n)]} \tag{A8}$$

where C is an integration constant defined by the value of p_c at time zero.

$$C = (p_{c,t=0}/p_0)^{(1-n)} - 1 \tag{A9}$$

References

[1]Lovine, R.L., Baum, J.D., and Levine, J.N., "Ejecta Pulsing of Subscale Solid Propellant Rocket Motors," *AIAA Journal*, Vol. 23, March 1985, pp. 416-423.

[2]Godunov, S.K., Zabrodyn, A.W., and Prokopov, G.P., "A Difference Scheme for Two-Dimensional Unsteady Problems of Gas Dynamics and Computation of Flow with a Detached Shock Wave," *Zhurnal Vychyslitelnoi: Matematiki i Mathematicheskoi Fiziki*, Vol. 1, Dec. 1961, p. 1020; also, Cornell Aerolab Translation (AD614916).

[3]Murdock, J.W., "Shock-Wave Interaction with Two-Dimensional Bodies," *AIAA Journal*, Vol. 13, Sept. 1975, pp. 1139-1140.

[4]Widhopf, G.F., Buell, J.C., and Schmidt, E.M., "Time-Dependent Near Field Muzzle Brake Flow Simulations," AIAA Paper 82-0973, June 1982.

[5]Heister, S.D. and Landsbaum, E.M., "Analysis of Ballistic Anomalies in Solid Rocket Motors," AIAA Paper 85-1303, July 1985.